Dynamic Impact Factors for Shear and Bending Moment of Simply Supported and Continuous Concrete Girder Bridges

Lu Deng, Ph.D., M.ASCE[1]; Wei He[2]; and Yi Shao[3]

Abstract: The girder bridge is one of the most popular bridge types throughout the world. Although much effort has been made to study the impact factor (IF) of simply supported bridges due to vehicle loading, fewer works have been reported on continuous bridges. In addition, most of the previous research on IFs has focused on the bending moment effect, whereas very few studies have focused on the shear effect. In this study, numerical simulations were performed to study the dynamic IFs of both simply supported and continuous bridges due to vehicle loading. IFs for both shear and bending moment were investigated. Some interesting findings were obtained regarding the relationships between the IFs of simply supported and continuous bridges, for both shear and bending moment. These findings can be used as additional references for bridge codes by practicing engineers. **DOI: 10.1061/(ASCE)BE.1943-5592.0000744.**

Author keywords: Dynamic impact factor; Simply supported bridge; Continuous bridge; Shear; Bending moment.

Introduction

The girder bridge is one of the most popular bridge types throughout the world. Numerous studies have been conducted to study the dynamic performance of girder bridges ever since the 1950s (Huang et al. 1992). A significant amount of effort has been made to study the impact factor (IM) of simply supported bridges due to vehicle loading (Shepherd and Aves 1973; Huang et al. 1992; Chang and Lee 1994; Deng and Cai 2010), whereas fewer studies have been reported on continuous bridges. Huang et al. (1992) studied the IM of six continuous multigirder steel bridges with different span lengths due to moving vehicles and found that the IM equation given in the AASHTO (1989) standard specifications may underestimate the impact at the interior supports for short bridges. Wang et al. (1996) also studied the dynamic behavior of three continuous and cantilever thin-wall box-girder bridges under vehicle loading. They found IMs much higher than the values specified in bridge codes when the vehicle speed reached 120 km/h (75 mi/h). Fafard et al. (1998), based on the analysis of existing continuous bridges, pointed out that the AASHTO (1994) standard specifications tend to underestimate the IMs for long-span continuous bridges. Shi et al. (2010), based on the IMs measured from 40 simply supported bridges and 26 continuous bridges, found that the IMs of continuous bridges can be notably larger than simply supported bridges with the same span lengths, especially for long bridges. They suggested that caution should be used when applying the IMs in the bridge code for evaluation of existing continuous bridges. However, the difference between the IMs for simply supported and continuous bridges is usually ignored in practice.

Additionally, most of the previous research on IMs has focused on the bending moment effect, whereas very few studies have focused on the shear effect. Although shear failures are not so frequent for bridges, immediate attention and accurate assessment of the applied shear force are needed if signs of cracking are seen close to the support (González et al. 2011). Yang et al. (1995) found that the IMs for shear could be larger than those for bending moment. However, González et al. (2011) studied the IMs for shear due to heavy vehicles crossing highway bridges and found that for short bridges, the mean IM for shear was smaller than that for bending moment. In addition, some bridge codes also treat the IMs for shear and bending moment differently. For example, in the European code (CEN 2003), the built-in dynamic amplification factor for shear for one-lane bridges is 0.2–0.3 less than that for bending moment depending on the span length. In the New Zealand Transport Agency (NZTA 2013) Bridge Manual, the dynamic load factor (DLF) for shear is given as a constant value of 1.30, whereas the DLF for moments in simple or continuous spans is specified as a function of the bridge span length. A review of the different IMs for bending moment and shear adopted by some bridge design codes can be found in Deng et al. (2014).

Many researchers have found that the IMs calculated from different bridge responses are different, and some have argued that the IMs obtained from different bridge responses should be treated differently (Wang et al. 1994; Huang et al. 1995; Fafard et al. 1998). However, the IMs were traditionally calculated using the bending moment or displacement and were usually not treated differently in bridge codes and in practice (Deng et al. 2014). It is, therefore, clear that more research is needed in order to gain a clearer understanding of the relationship between the IMs for different bridge types and bridge responses and to use them more properly in engineering practice (Deng et al. 2014).

In this study, numerical simulations were performed to study the IMs of six concrete girder bridges, including four simply supported bridges and two three-span continuous bridges, due to vehicle loading. The IMs for both shear and bending moment were investigated. Some interesting findings were obtained regarding the

[1]Professor, College of Civil Engineering, Hunan Univ., Changsha, Hunan 410082, China (corresponding author). E-mail: denglu@hnu.edu.cn

[2]Research Assistant, College of Civil Engineering, Hunan Univ., Changsha, Hunan 410082, China. E-mail: hewei.hnu@gmail.com

[3]Research Assistant, College of Civil Engineering, Hunan Univ., Changsha, Hunan 410082, China. E-mail: alexandersysz@gmail.com

Note. This manuscript was submitted on July 23, 2014; approved on November 12, 2014; published online on March 10, 2015. Discussion period open until August 10, 2015; separate discussions must be submitted for individual papers. This paper is part of the ***Journal of Bridge Engineering***, © ASCE, ISSN 1084-0702/04015005(9)/$25.00.

relationships between the IMs for simply supported and continuous bridges and the IMs for shear and bending moment. These findings can be used as additional references for bridge codes by practicing engineers.

Numerical Bridge and Vehicle Models

Bridge Model

In the present study, six concrete girder bridges, including three T-girder bridges and three box-girder bridges, were studied. Each type of girder bridge includes two simply supported bridges and one continuous bridge. All three bridges with the same type of girder have the same cross section. Fig. 1 shows the cross section of the two types of girders. Some brief information on the six bridges is also provided in Table 1.

To calculate the IMs, bridge responses at different locations were selected. For the simply supported bridges, the bending moments at the midspan and the shear at the end supports were used. For the continuous bridges, the sections selected for calculating the IMs are illustrated in Fig. 2. Owing to the geometric symmetry of the bridge, only sections from the left half of the bridges were selected, as shown in Fig. 2. For the bending moment, the sections where the maximum positive moment occurs (P1 and P2), and where the maximum negative moment occurs (N1), were selected. For shear, sections close to the supports, namely, S1 for the end support and S2 for the first interior support, were selected. It should be noted that section S2 (on the right of the interior support) has larger shear strain than the corresponding section on the left of the interior support shown in Fig. 2. Therefore, only S2 was selected for this interior support. In addition, the sections for shear are both 0.6 m away from the support to reduce the influence of the support on the shear strain, as was done by Yang et al. (2004).

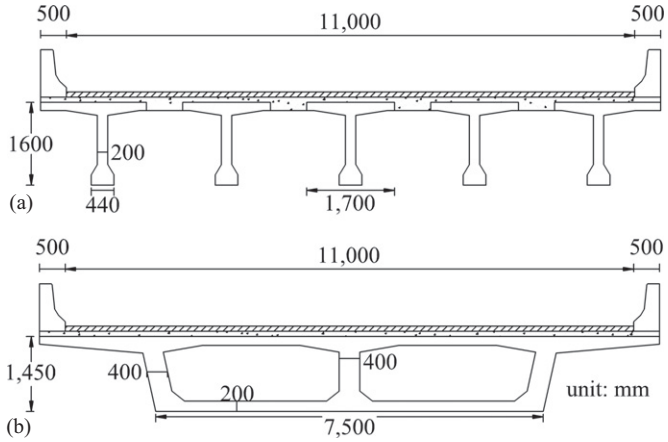

Fig. 1. Cross section of the two types of concrete girder bridges: (a) T-girder; (b) box-girder

Vehicle Model

The HS20-44 truck used in the AASHTO (2012) bridge design specifications was adopted for the vehicle loading in this study. An analytical model was developed for this truck, as shown in Fig. 3. This truck model consists of 11 independent degrees of freedom. The detailed geometric and mechanical properties of the truck are shown in Table 2 (Wang and Huang 1992). The modal frequencies of the vehicle were calculated as 1.52, 2.14, 2.69, 5.94, 7.74, 7.82, 8.92, 13.87, 13.99, 14.63, and 17.95 Hz, respectively.

Road Roughness Profile

Road surface irregularity is regarded as a main cause of the dynamic effect of moving vehicles in the AASHTO (2012) LRFD code. An artificial road profile is generally represented by a zero-mean stationary random process that can be expressed by a power spectral density (PSD) function. In this study, a modified PSD function (Huang et al. 1992) was used

$$\varphi(n) = \varphi(n_0)\left(\frac{n}{n_0}\right)^{-2} \quad (n_1 < n < n_2) \tag{1}$$

where n = spatial frequency (cycle/m); n_0 = discontinuity frequency of 0.5π (cycle/m); $\varphi(n_0)$ = roughness coefficient (m^3/cycle); and n_1 and n_2 = lower and upper cutoff frequencies, respectively. The International Organization for Standardization (ISO 1995) classified the road surface condition (RSC) based on different values of roughness coefficient. Three different RSCs, namely, good, average, and poor, according to the ISO, were considered in the present study. The corresponding roughness coefficients used were 20×10^{-6}, 80×10^{-6}, and 256×10^{-6} m^3/cycle for good, average, and poor RSCs, respectively, which can also be found in Kong et al. (2014).

With the PSD function, the road surface profile can then be generated by an inverse Fourier transform as follows:

$$r(x) = \sum_{k=1}^{N} \sqrt{2\varphi(n_k)\Delta n} \cos(2\pi n_k x + \theta_k) \tag{2}$$

where θ_k = random phase angle uniformly distributed from 0 to 2π; n_k = wave number (cycle/m); N = number of frequencies between n_1 and n_2; and Δn = frequency interval between n_1 and n_2 divided by N.

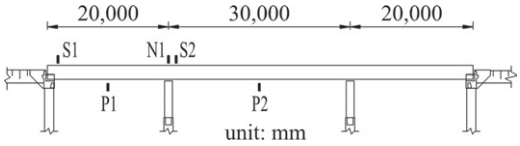

Fig. 2. Sections selected on the continuous bridges for calculating the impact factors

Table 1. Brief Information on the Six Bridges Used in This Study

Girder type	Symbol	Bridge type	Span length (m)	Natural frequency (Hz)
T-girder	T20	Simply supported	20	5.88
	T30	Simply supported	30	2.69
	T70	Continuous	20 + 30 + 20	4.86
Box-girder	B20	Simply supported	20	6.79
	B30	Simply supported	30	3.14
	B70	Continuous	20 + 30 + 20	5.11

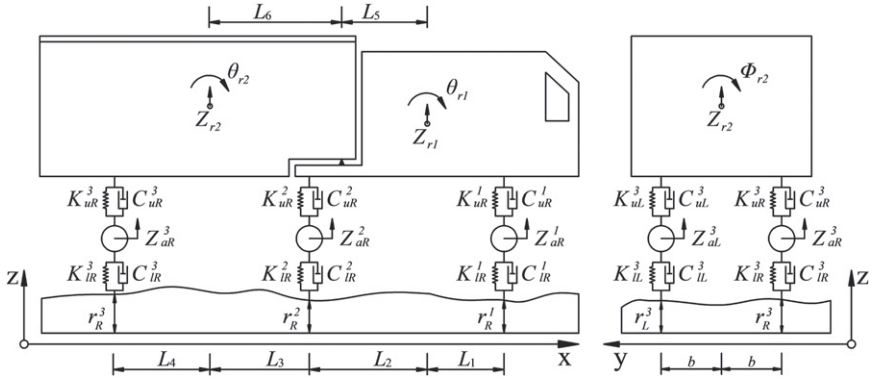

Fig. 3. Analytical model of the HS20-44 truck

Table 2. Major Parameters of the HS20-44 Truck

Items	Parameters	Values
Geometry	L1	1.698 (m)
	L2	2.569 (m)
	L3	1.984 (m)
	L4	2.283 (m)
	L5	2.215 (m)
	L6	2.338 (m)
	b	1.1 (m)
Mass	Truck body 1	2,612 (kg)
	Truck body 2	26,113 (kg)
	First axle suspension	490 (kg)
	Second axle suspension	808 (kg)
	Third axle suspension	653 (kg)
Moment of inertia	Pitching, truck body 1	2,022 (kg/m^2)
	Rolling, truck body 1	8,544 (kg/m^2)
	Pitching, truck body 2	33,153 (kg/m^2)
	Rolling, truck body 2	181,216 (kg/m^2)
Spring stiffness	Upper, first axle	242,604 (N/m)
	Lower, first axle	875,082 (N/m)
	Upper, second axle	1,903,172 (N/m)
	Lower, second axle	3,503,307 (N/m)
	Upper, third axle	1,969,034 (N/m)
	Lower, third axle	3,507,429 (N/m)
Damper coefficient	Upper, first axle	2,190 (N·s/m)
	Lower, first axle	2,000 (N·s/m)
	Upper, second axle	7,882 (N·s/m)
	Lower, second axle	2,000 (N·s/m)
	Upper, third axle	7,182 (N·s/m)
	Lower, third axle	2,000 (N·s/m)

Bridge–Vehicle Coupled System

The two sets of equations of motion for the vehicle and bridge can be written in a matrix form as follows:

$$[M_v]\{\ddot{d}_v\} + [C_v]\{\dot{d}_v\} + [K_v]\{d_v\} = \{F_G\} + \{F_v\} \tag{3}$$

$$[M_b]\{\ddot{d}_b\} + [C_b]\{\dot{d}_b\} + [K_b]\{d_b\} = \{F_b\} \tag{4}$$

where $[M_v]$, $[C_v]$, and $[K_v]$ = mass, damping, and stiffness matrices of the vehicle, respectively; $[M_b]$, $[C_b]$, and $[K_b]$ = mass, damping, and stiffness matrices of the bridge, respectively; $\{d_v\}$ and $\{d_b\}$ = displacement vectors of the vehicle and bridge, respectively; $\{F_G\}$ = gravity force vector of the vehicle; and $\{F_v\}$ and $\{F_b\}$ = wheel–road contact force vector acting on the vehicle and bridge, respectively. Given the displacement relationship and the interaction force relationship at the contact points, the two sets of equations of motion above can be combined into one coupled equation

$$\begin{bmatrix} M_b & \\ & M_v \end{bmatrix} \begin{Bmatrix} \ddot{d}_b \\ \ddot{d}_v \end{Bmatrix} + \begin{bmatrix} C_b + C_{b-b} & C_{b-v} \\ C_{v-b} & C_v \end{bmatrix} \begin{Bmatrix} \dot{d}_b \\ \dot{d}_v \end{Bmatrix} + \begin{bmatrix} K_b + K_{b-b} & K_{b-v} \\ K_{v-b} & K_v \end{bmatrix} \begin{Bmatrix} d_b \\ d_v \end{Bmatrix} = \begin{Bmatrix} F_{b-r} \\ F_{b-r} + F_G \end{Bmatrix} \tag{5}$$

where C_{b-b}, C_{b-v}, C_{v-b}, K_{b-b}, K_{b-v}, K_{v-b}, F_{b-r}, and F_{b-r} = terms due to the interaction between the bridge and vehicle. These interaction terms are time-dependent and will change as the vehicle moves across the bridge.

To reduce the size of matrices and save computational efforts, the modal superposition technique was used and Eq. (5) can then be simplified as follows:

$$\begin{bmatrix} I & \\ & M_v \end{bmatrix} \begin{Bmatrix} \ddot{\xi}_b \\ \ddot{d}_v \end{Bmatrix} + \begin{bmatrix} 2\omega_i\eta_i I + \Phi_b{}^T C_{b-b}\Phi_b & \Phi_b{}^T C_{b-v} \\ C_{v-b}\Phi_b & C_v \end{bmatrix} \begin{Bmatrix} \dot{\xi}_b \\ \dot{d}_v \end{Bmatrix} + \begin{bmatrix} \omega_i{}^2 I + \Phi_b{}^T K_{b-b}\Phi_b & \Phi_b{}^T K_{b-v} \\ K_{v-b}\Phi_b & K_v \end{bmatrix} \begin{Bmatrix} \xi_b \\ d_v \end{Bmatrix} = \begin{Bmatrix} \Phi_b{}^T F_{b-r} \\ F_{v-r} + F_G \end{Bmatrix} \tag{6}$$

A computer program was developed using *MATLAB* to assemble the matrices into Eq. (6), which was then solved by using the fourth-order Runge–Kutta method in the time domain. For more details about the derivation of Eq. (6) and the solving process, readers can refer to Deng and Cai (2009). The developed bridge–vehicle coupled model has also been validated using field measurements by Cai et al. (2007) and Deng and Cai (2011).

With the obtained displacement responses of the bridge $\{d_b\}$, the strain responses can be obtained by

$$\{\varepsilon\} = [B]\{d_b\} \tag{7}$$

where $[B]$ = strain–displacement relationship matrix assembled with x, y, and z derivatives of the element shape functions.

The dynamic IM, also known as the dynamic load allowance (DLA), is calculated as follows:

$$\text{IM} = \frac{R_{dyn} - R_{sta}}{R_{sta}} \tag{8}$$

where R_{dyn} and R_{sta} = maximum dynamic and static responses of the bridge, respectively.

Numerical Simulation Results

A comprehensive study on the effect of different parameters on the IMs was conducted in this study. Seven vehicle speeds ranging from 15 to 120 km/h were investigated. Three RSCs were considered, namely, good, average, and poor. A loading scenario with two trucks traveling across the bridge side by side was used. The loading position of the trucks is shown in Fig. 4.

To reduce the bias due to the randomness of the generated road surface profile, for each combination of different parameters including a certain RSCs, 20 random road surface profiles were generated and the bridge–vehicle coupled system was set to run 20 times independently, resulting in 20 IMs. The average of the 20 IMs was then used in the result analysis.

The IMs for bending moment are plotted against vehicle speed for the T-girder bridges and box-girder bridges in Fig. 5 and Fig. 6, respectively. Figs. 5 and 6 show the following:

1. The variation of IMs with vehicle speed does not follow a specific trend, which has also been reported by many other researchers (Broquet et al. 2004; Deng and Cai 2010; Ashebo et al. 2007; Azimi et al. 2011). Although many researchers have attempted to explain this phenomenon, a convincing explanation is still lacking, owing to the fact that vehicle-induced vibration is very complicated and influenced by a large number of different factors at the same time (Deng et al. 2014).
2. The IMs for negative bending moment at the interior supports (N1) are larger than those for positive bending moment at the midspan (P1 and P2), which was also reported by Huang et al. (1992). This suggests that proper caution should be used when using IMs in designing or evaluating the negative bending moment of continuous bridges at their interior supports.
3. The IMs for positive bending moment at the side span (P1) are larger than those at the center span (P2) and also those of simply supported bridges with the same span length (T20 and B20). Huang et al. (1992) concluded that this could be due to the fact that the impact of the side span was principally affected by high modes and they attempted to use an equivalent shorter span length to explain the larger IMs. However, it should be noted that both numerical simulation and field test results suggest that longer span lengths do not necessarily guarantee smaller IMs (Cantieni 1983; Coussy et al. 1989; Deng and Cai 2010).
4. The IMs all fall below 0.33 as specified in the current AASHTO (2012) LRFD code when the RSC is good. However, the IMs for negative bending moment at the interior supports exceed 0.33 in most cases with average RSC, and IMs at all selected sections can exceed 0.33 at certain vehicle

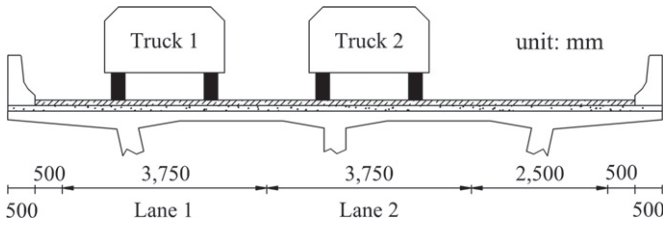

Fig. 4. Loading position of the trucks

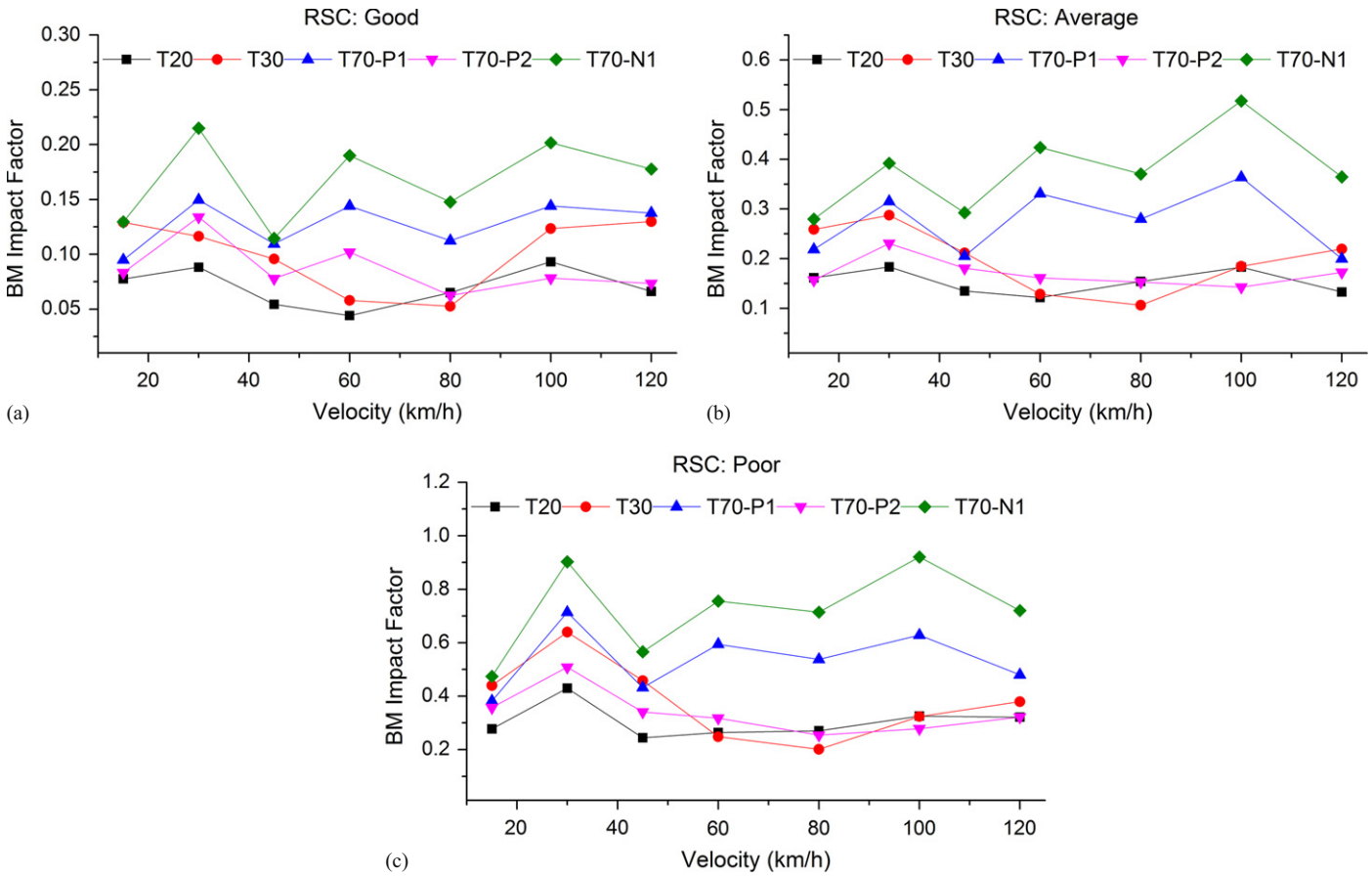

Fig. 5. Impact factors for bending moment of the T-girder bridges: (a) good RSC; (b) average RSC; (c) poor RSC

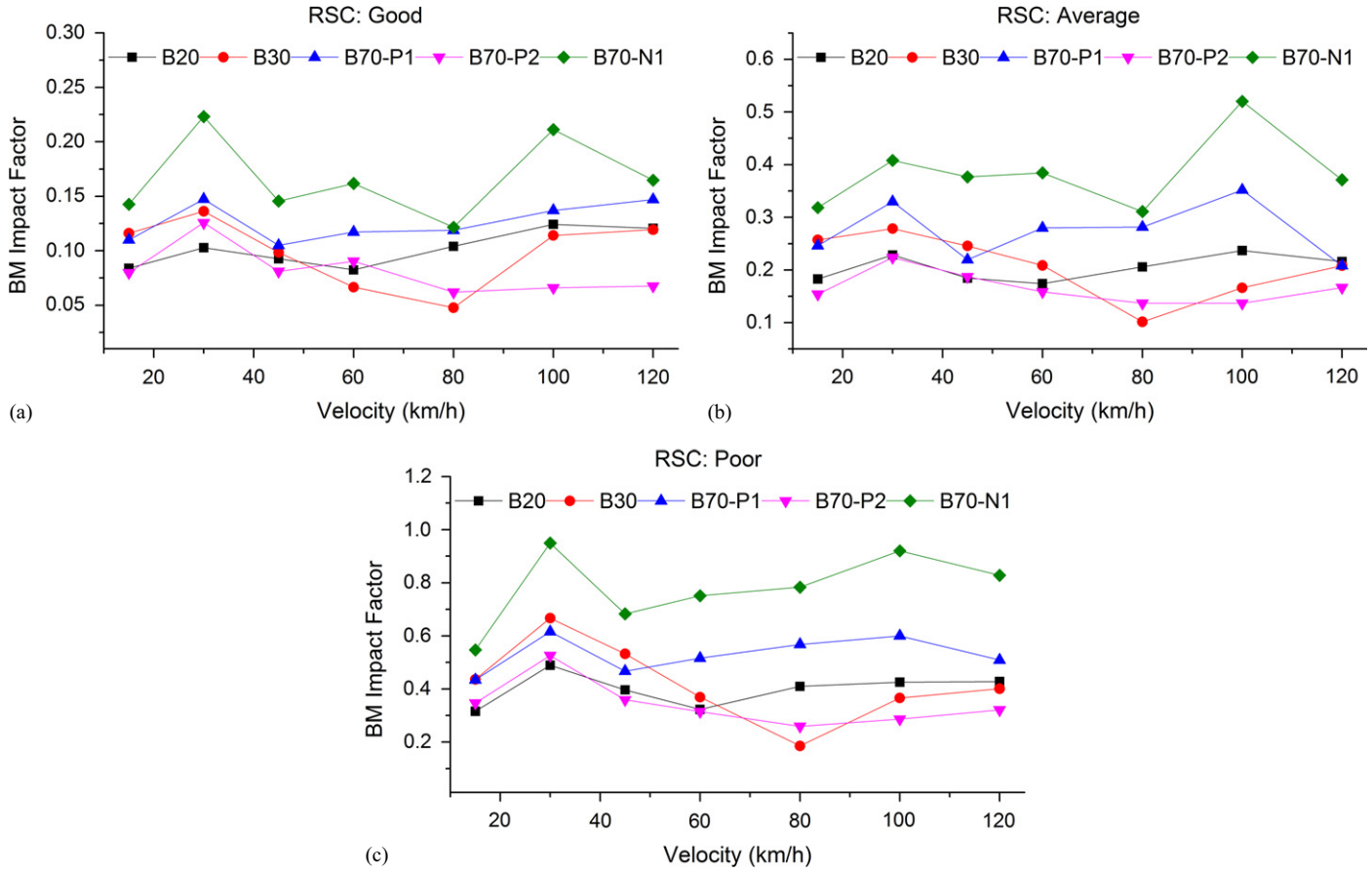

Fig. 6. Impact factors for bending moment of the box-girder bridges: (a) good RSC; (b) average RSC; (c) poor RSC

speeds when the RSC becomes poor. These results suggest that maintaining a regular maintenance program for the RSC can be a very effective way to reduce the impact of bridges due to vehicle loading.

The IMs for shear are also plotted against vehicle speed for different sections of the T-girder bridges and box-girder bridges in Fig. 7 and Fig. 8, respectively. The following can be observed from Figs. 7 and 8:

1. Similar to the IMs for bending moment, the IMs for shear do not follow a specific trend with the variation of vehicle speed.
2. The shear IMs of continuous bridges are larger than those of simply supported bridges in most cases, for both T-girder and box-girder bridges. The shear IMs at the end support (S1) and the interior support (S2) of the continuous bridges are larger than those at the end supports of the simply supported bridges with the same span lengths of 20 and 30 m, respectively.
3. The shear IMs at the end support (S1) are larger than those at the interior support (S2) in most cases, whereas the shear strain at the end support (S1) is smaller than that at the interior support (S2). This may indicate that larger shear strains lead to smaller IMs. Similar results were also reported by Huang et al. (1992).
4. The shear IMs are all <0.33 when the RSC is average or good, whereas they are generally >0.33 when the RSC is poor.

To investigate the relationship between the IMs for bending moment and shear, the IMs for the simply supported bridges and continuous bridge were compared. The IMs of the side span (with a span length of 20 m) of the continuous bridges and the 20-m-long simply supported bridges are plotted against the RSC in Fig. 9, and the IMs of the center span (with a span length of 30 m) of the continuous bridges and the 30-m-long simply supported bridges are plotted in Fig. 10. Quantitative comparisons between the IMs of the continuous bridges and simply supported bridges were also made, as shown in Table 3. In Figs. 9 and 10, in addition to the mean values, the standard deviations of the IMs are also included, as indicated by the lengths of the bars in the vertical direction. The following can be observed from the analysis of the results:

1. As can be seen in Figs. 9 and 10, as the RSC changes from good to poor, the IMs increase significantly from <0.1 to >0.4 in some cases; for good and average RSCs, the average IMs for shear and bending moment, for both simply supported and continuous bridges, are all far below 0.33, the value specified in the AASHTO (2012) code; however, under poor RSCs, the average IMs are all larger than 0.33. In addition, the standard deviation of the IMs increases significantly as the RSC becomes worse.
2. The bending moment IMs at the center span of the continuous bridges are all smaller than those of the simply supported bridges with the same span length of 30 m, as shown in Table 3. In contrast, the bending moment IMs at the side span of the continuous bridges are all larger than those of the simply supported bridges with the same span length of 20 m.
3. Unlike the IMs for bending moment, the shear IMs for the continuous bridges are all larger than those of the simply supported bridges with the same span length, as shown in

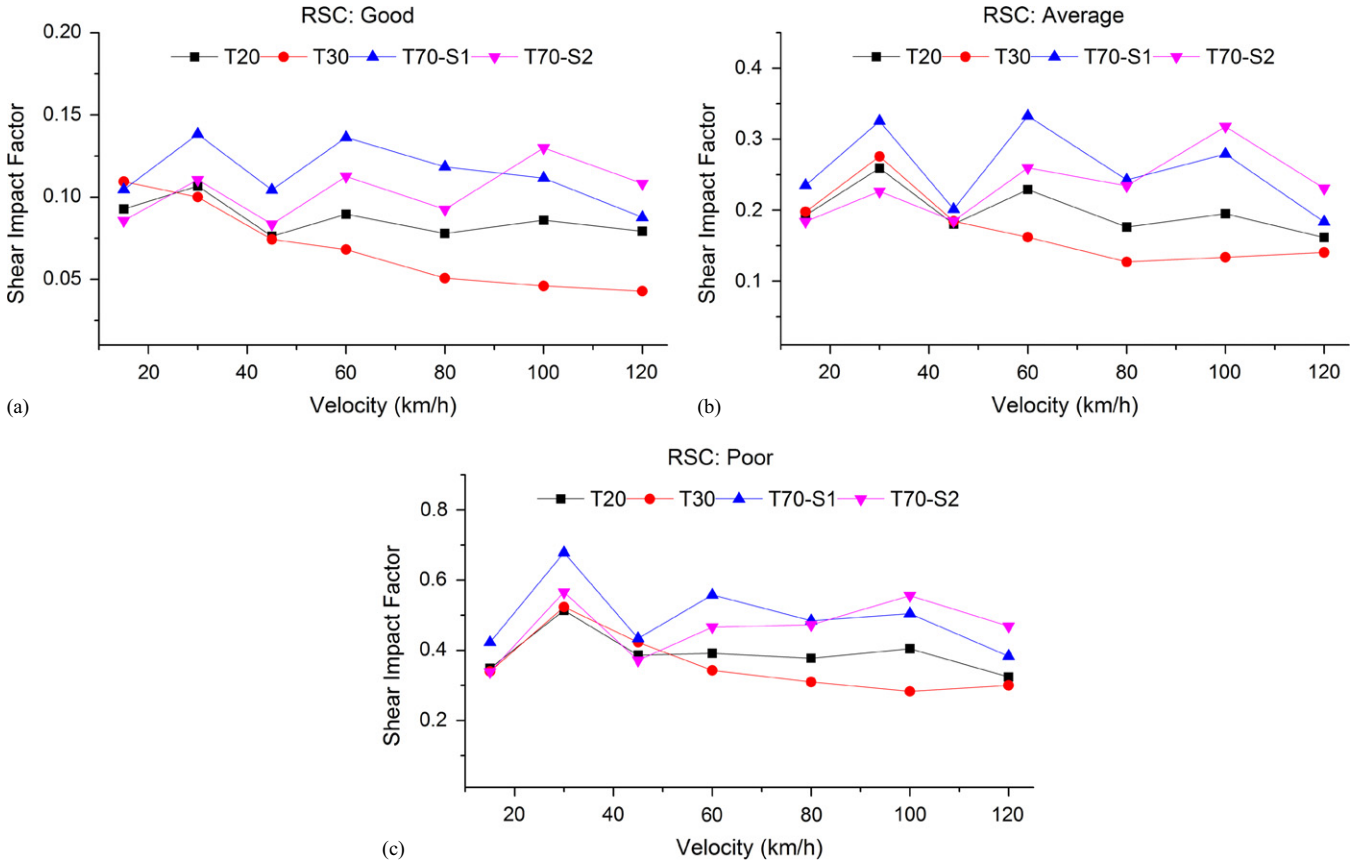

Fig. 7. Impact factors for shear of the T-girder bridges: (a) good RSC; (b) average RSC; (c) poor RSC

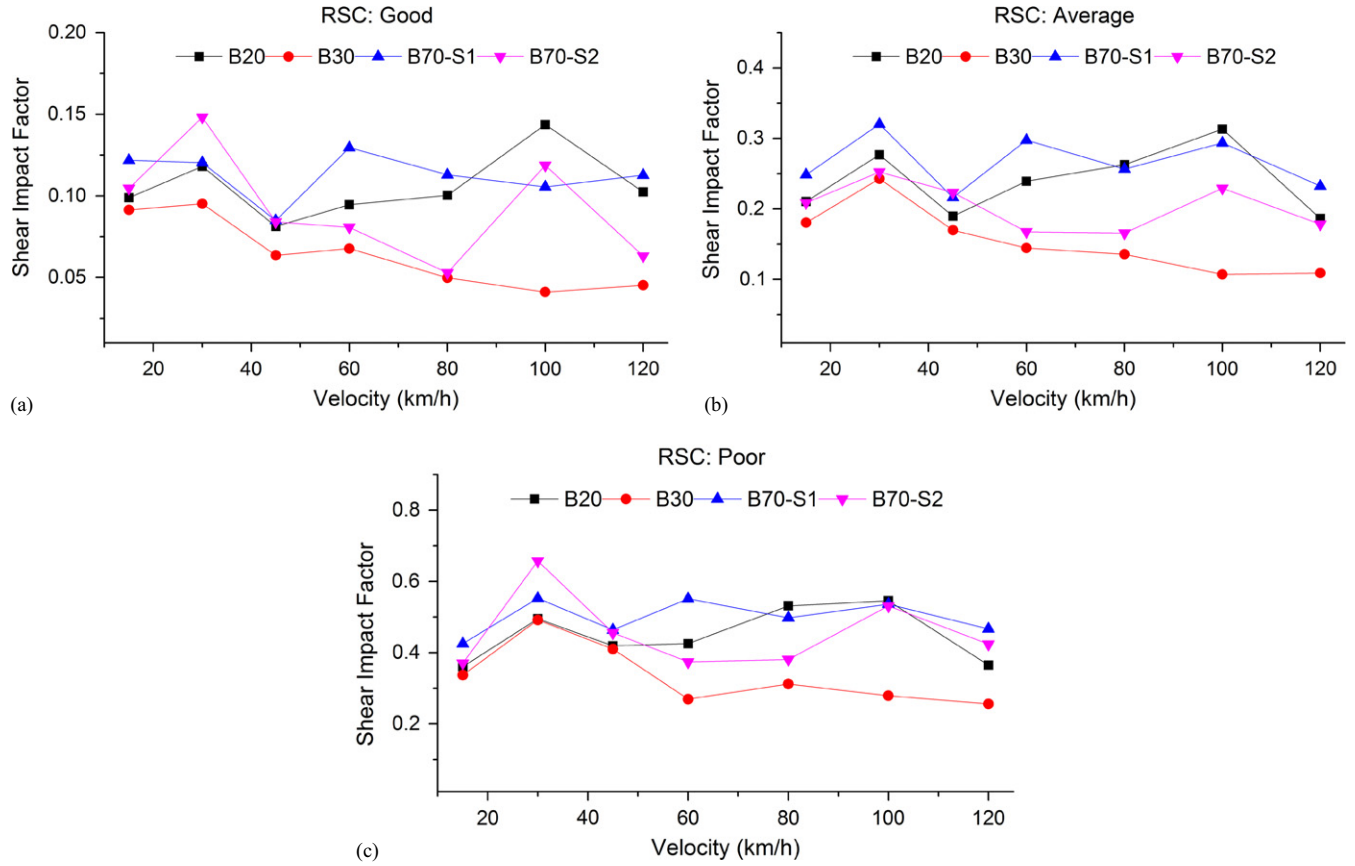

Fig. 8. Impact factors for shear of the box-girder bridges: (a) good RSC; (b) average RSC; (c) poor RSC

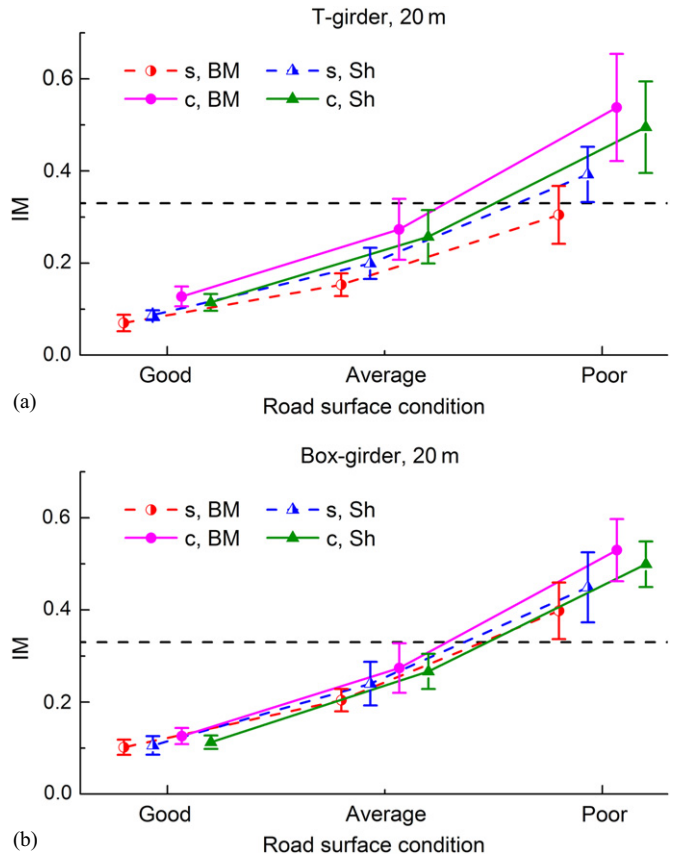

Fig. 9. Mean and standard deviation of impact factors of the side span of the continuous bridges and corresponding simply supported bridges with span length of 20 m: (a) T-girder; (b) box-girder; in the figure, s—simply supported; c—continuous; BM—bending moment; Sh—shear

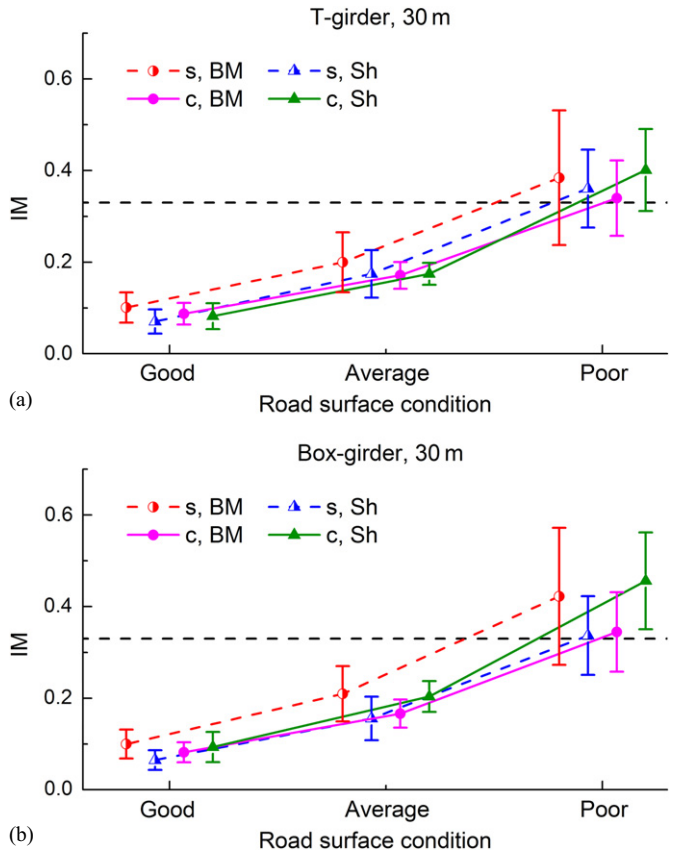

Fig. 10. Mean and standard deviation of impact factors of the center span of the continuous bridges and corresponding simply supported bridges with a span length of 30 m: (a) T-girder; (b) box-girder; in the figure, s—simply supported; c—continuous; BM—bending moment; Sh—shear

Table 3. This trend is very clear for box-girder bridges with the average relative difference reaching over 35%.

4. It is also interesting to note from the results that no concluding relationships could be observed between the IMs for bridges with different girder cross sections. For example, for the bending moment, there are only slight differences between the IMs for T-girder bridges and box-girder bridges, for both simply supported bridges and continuous bridges, whereas for shear, the differences are significant. Further investigation on a larger number of bridge samples may be needed to uncover the complicated relationship between the IMs for bridges with different cross sections.

Resonance between the bridge and vehicle is probably the cause for the different observations of the bending moment IMs presented in the previous section. It is noted that the fourth vibration frequency of the continuous T-girder bridge (8.60 Hz) and the second vibration frequency of the continuous box-girder bridge (7.93 Hz) are very close to the seventh and fifth vibration frequencies of the vehicle (8.92 and 7.74 Hz), which correspond to the hopping of the second and first axles of the vehicle, respectively. From Figs. 11 and 12, it can be seen that these two vibration modes (one for each bridge) have the largest contribution, among the first four vibration modes, to the bending moment of the side span of each corresponding bridge. As for the corresponding simply supported bridges with a span length of 20 m, the natural frequency of the T-girder bridge (5.88 Hz) is close to the fourth vibration mode of the vehicle (5.94 Hz), which, however, corresponds to the tractor-rolling mode and has little contribution

Table 3. Comparison of Impact Factors for Continuous and Simply Supported Bridges $((IM_{conti} - IM_{simp})/IM_{simp})$

		Span: 20 m (side span)		Span: 30 m (center span)	
Girder type	RSC	Bending moment (BM) (%)	Shear (Sh) (%)	Bending moment (BM) (%)	Shear (Sh) (%)
T	Good	82.6	31.7	– 13.3	16.7
	Average	78.6	29.1	– 14.3	0.1
	Poor	76.6	26.2	– 11.6	11.3
Box	Good	24.2	6.6	– 18.0	43.7
	Average	34.2	11.1	– 20.6	30.8
	Poor	33.1	11.2	– 18.4	35.5

to the midspan bending moment. The natural frequency of the box-girder bridge (6.79 Hz), on the other hand, is not close to any vehicle vibration mode. As a result, the bending moment IMs at the side span of the continuous bridges are larger than those at the midspan of the corresponding simply supported bridges.

For the center span of 30 m, the first vibration mode has a significant contribution to the bending moment of the center span for both continuous bridges, as illustrated in Figs. 11 and 12. However, the first vibration frequencies of 4.86 and 5.11 Hz, for the T-girder and box-girder bridges, respectively, are not close to any vibration frequency of the vehicle. Nonetheless, the natural frequencies of the 20-m-long simply supported bridges (2.69 Hz for the T-girder bridge and 3.14 Hz for the box-girder bridge) are close to the third vibration frequency (2.68 Hz), which

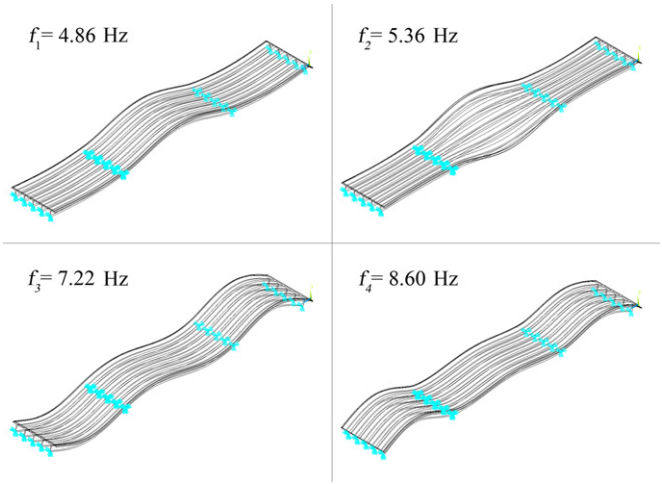

Fig. 11. First four modes of the continuous T-girder bridge

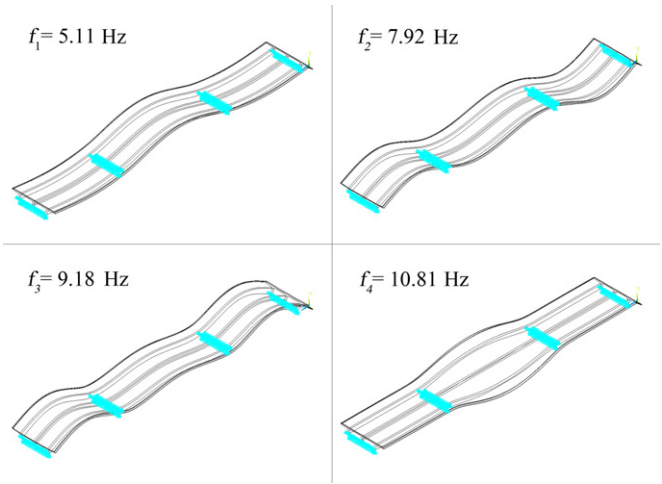

Fig. 12. First four modes of the continuous box-girder bridge

corresponds to the tractor-pitching mode of the vehicle. As a result, the bending moment IMs at the center span of the continuous bridges are smaller than those at the midspan of the corresponding simply supported bridges.

A main reason why the shear IMs of the continuous bridges are larger than those of the corresponding simply supported bridges could be that the shear strains on the continuous bridges were generally found to be smaller than those on the simply supported bridges. It is generally believed that larger responses usually lead to smaller IMs (Huang et al. 1992, 1993; Cai et al. 2007).

Concluding Remarks

The IM of simply supported and continuous bridges due to vehicle loading was studied in this paper. IMs for both shear and bending moment were investigated. Given the comparisons of the obtained IMs from this study, the following findings can be obtained:

1. The IMs for negative bending moment of the continuous bridges are larger than those for positive bending moment.
2. For the bridges studied, it is found that the bending moment IMs at the center span of the continuous bridges are smaller than those of the simply supported bridges with the same span length, whereas the bending moment IMs at the side span of the continuous bridges are larger than those of the simply supported bridges with the same span length. An in-depth investigation reveals that the resonance between the bridge and vehicle is probably the cause for this phenomenon.
3. The shear IMs of the continuous bridges are larger than those of the simply supported bridges with the same span length.

The findings from this study suggest that in strength design or capacity evaluation of continuous girder bridges, the use of IMs calculated from the responses of simply supported bridges may not be appropriate or safe. Besides, the IMs for bending moment and shear should be treated differently. The results from this study can be used as additional references for current bridge codes by bridge engineers and researchers when dealing with related matters. It should be noted, however, that the findings in this study were based on the numerical studies on a few bridges with certain span lengths, and are of a more qualitative nature than quantitative. More comprehensive numerical studies or field tests on more bridge samples with a wider range of span lengths are suggested in order to draw more comprehensive and general conclusions that can be used in bridge codes.

Acknowledgments

The authors gratefully acknowledge the financial support provided by the National Natural Science Foundation of China (Grant No. 51208189 and 51478176) and Excellent Youth Foundation of Hunan Scientific Committee (Grant No. 14JJ1014).

References

AASHTO. (1989). *Standard specifications for highway bridges*, Washington, DC.
AASHTO. (1994). *Standard specifications for highway bridges*, Washington, DC.
AASHTO. (2012). *LRFD bridge design specifications*, Washington, DC.
Ashebo, D. B., Chan, T. H. T., and Yu, L. (2007). "Evaluation of dynamic loads on a skew box girder continuous bridge. Part II: Parametric study and dynamic load factor." *Eng. Struct.*, 29(6), 1064–1073.
Azimi, H., Galal, K., and Pekau, O. A. (2011). "A modified numerical VBI element for vehicles with constant velocity including road irregularities." *Eng. Struct.*, 33(7), 2212–2220.
Broquet, C., Bailey, S. F., Fafard, M., and Brühwiler, E. (2004). "Dynamic behavior of deck slabs of concrete road bridges." *J. Bridge Eng.*, 10.1061/(ASCE)1084-0702(2004)9:2(137), 137–146.
Cai, C. S., Shi, X. M., and Araujo, M. (2007). "Effect of approach span condition on vehicle-induced dynamic response of slab-on-girder road bridges." *Eng. Struct.*, 29(12), 3210–3226.
Cantieni, R. (1983). "Dynamic load tests on highway bridges in Switzerland-60 years of experience of EMPA." *EMPA Rep. No. 211*, Swiss Federal Laboratories for Materials Testing and Research, Dübendorf, Switzerland.
CEN (European Committee for Standardization). (2003). *Eurocode 1: Actions on structures—part 2: Traffic loads on bridges*, Brussels, Belgium.
Chang, D., and Lee, H. (1994). "Impact factors for simple-span highway girder bridges." *J. Struct. Eng.*, 10.1061/(ASCE)0733-9445(1994)120:3(704), 704–715.
Coussy, O., Said, M., and van Hoove, J. P. (1989). "The influence of random surface irregularities on the dynamic response of bridges under suspended moving loads." *J. Sound Vib.*, 130(2), 313–320.
Deng, L., and Cai, C. S. (2009). "Identification of parameters of vehicles moving on bridges." *Eng. Struct.*, 31(10), 2474–2485.

Deng, L., and Cai, C. S. (2010). "Development of dynamic impact factor for performance evaluation of existing multi-girder concrete bridges." *Eng. Struct.*, 32(1), 21–31.

Deng, L., and Cai, C. S. (2011). "Identification of dynamic vehicular axle loads: Demonstration by a field study." *J. Vib. Control*, 17(2), 183–195.

Deng, L., Yu, Y., Zou, Q. L., and Cai, C. S. (2014). "State-of-the-art review on dynamic impact factors of highway bridges". *J. Bridge Eng.*, 10.1061/(ASCE)BE.1943-5592.0000672, 04014080.

Fafard, M., Laflamme, M., Savard, M., and Bennur, M. (1998). "Dynamic analysis of existing continuous bridge." *J. Bridge Eng.*, 10.1061/(ASCE)1084-0702(1998)3:1(28), 28–37.

González, A., Cantero, D., and OBrien, E. J. (2011). "Dynamic increment for shear force due to heavy vehicles crossing a highway bridge." *Comput. Struct.*, 89(23–24), 2261–2272.

Huang, D., Wang, T. L., and Shahawy, M. (1992). "Impact analysis of continuous multigirder bridges due to moving vehicles." *J. Struct. Eng.*, 10.1061/(ASCE)0733-9445(1992)118:12(3427), 3427–3443.

Huang, D., Wang, T. L., and Shahawy, M. (1993). "Impact studies of multigirder concrete bridges." *J. Struct. Eng.*, 10.1061/(ASCE)0733-9445(1993)119:8(2387), 2387–2402.

Huang, D., Wang, T. L., and Shahawy, M. (1995). "Vibration of thin walled box-girder bridges excited by vehicles." *J. Struct. Eng.*, 10.1061/(ASCE)0733-9445(1995)121:9(1330), 1330–1337.

ISO. (1995). "Mechanical vibration–road surface profiles–reporting of measured data." *ISO 8608: 1995(E)*, Geneva, Switzerland.

Kong, X., Cai, C. S., and Kong, B. (2014). "Damage detection based on transmissibility of a vehicle and bridge coupled system." *J. Eng. Mech.*, 10.1061/(ASCE)EM.1943-7889.0000821, 04014102.

NZTA (New Zealand Transport Agency). (2013). *Bridge manual*, Wellington, New Zealand.

Shepherd, R., and Aves, R. J. (1973). "Impact factors for simple concrete bridge." *Proc. Inst. Civil Eng.*, 55(1), 191–210.

Shi, S. W., Zhao, J., and Shu, S. Y. (2010). "Analysis of difference between measured value and code specified value for impact coefficient of girder bridge." *World Bridges*, 2(2), 79–82 (in Chinese).

Wang, T. L., and Huang, D. (1992). "Computer modeling analysis in bridge evaluation." *Research Rep. No. FLIDOTIRMCI0542-3394*, Florida Dept. of Transportation, Tallahassee, FL.

Wang, T. L., Huang, D., and Shahawy, M. (1994). "Dynamic behavior of slant-legged rigid-frame highway bridge." *J. Struct. Eng.*, 10.1061/(ASCE)0733-9445(1994)120:3(885), 885–902.

Wang, T. L., Huang, D., and Shahawy, M. (1996). "Dynamic behavior of continuous and cantilever thin-walled box girder bridges." *J. Bridge Eng.*, 10.1061/(ASCE)1084-0702(1996)1:2(67), 67–75.

Yang, Y. B., Liao, S. S., and Lin, B. H. (1995). "Impact formulas for vehicles moving over simple and continuous beams." *J. Struct. Eng.*, 10.1061/(ASCE)0733-9445(1995)121:11(1644), 1644–1650.

Yang, Y. B., Yau, J. D., and Wu, Y. S. (2004). *Vehicle bridge interaction dynamics: With application to high speed railways*, World Scientific, London.